

# On Orbit Performance of the MIPS Instrument

G. H. Rieke<sup>a</sup>, E. T. Young<sup>a</sup>, J. Cadien<sup>a</sup>, C. W. Engelbracht<sup>a</sup>, K. D. Gordon<sup>a</sup>, D. M. Kelly<sup>a</sup>, F. J. Low<sup>a</sup>, K. A. Misselt<sup>a</sup>, J. E. Morrison<sup>a</sup>, J. Muzerolle<sup>a</sup>, G. Rivlis<sup>a</sup>, J. A. Stansberry<sup>a</sup>, J. W. Beeman<sup>b</sup>, E. E. Haller<sup>b,i</sup>, D. T. Frayer<sup>c</sup>, W. B. Latter<sup>c</sup>, A. Noriega-Crespo<sup>c</sup>, D. L. Padgett<sup>c</sup>, D. C. Hines<sup>d</sup>, Doug Bean<sup>e</sup>, W. Burmester<sup>e</sup>, G. B. Heim<sup>e</sup>, Tom Glenn<sup>e</sup>, R. Ordonez<sup>e</sup>, J. P. Schwenker<sup>e</sup>, S. Siewert<sup>e</sup>, D. W. Strecker<sup>e</sup>, S. Tennant<sup>e</sup>, J. Troeltzsch<sup>e</sup>, B. Unruh<sup>e</sup>, R. M. Warden<sup>e</sup>, P. A. R. Ade<sup>f</sup>, A. Alonso-Herrero<sup>g</sup>, M. Blaylock<sup>a</sup>, H. Dole<sup>h</sup>, E. Egami<sup>a</sup>, J. L. Hinz<sup>a</sup>, E. Le Floc'h<sup>a</sup>, C. Papovich<sup>a</sup>, P. G. Pérez-González<sup>a</sup>, M. J. Rieke<sup>a</sup>, P. S. Smith<sup>a</sup>, K. Y. L. Su<sup>a</sup>, L. Bennett<sup>c</sup>, D. Henderson<sup>c</sup>, N. Lu<sup>c</sup>, F. Masci<sup>c</sup>, M. Pesenson<sup>c</sup>, L. Rebull<sup>c</sup>, J. Rho<sup>c</sup>, J. Keene<sup>c</sup>, S. Stolovy<sup>c</sup>, S. Wachter<sup>c</sup>, W. Wheaton<sup>c</sup>, P. L. Richards<sup>i</sup>, Harry Garner<sup>e</sup>, M. Hegge<sup>e</sup>, M. L. Henderson<sup>e</sup>, K. MacFeely<sup>e</sup>, D. Michika<sup>e</sup>, C. D. Miller<sup>e</sup>, M. Neitenbach<sup>e</sup>, J. Winghart<sup>e</sup>, R. Woodruff<sup>e</sup>, E. Arens, C. Beichman<sup>l</sup>, S. Gaalema<sup>k</sup>, T. N. Gautier<sup>l</sup>, C. Lada<sup>m</sup>, J. Mould<sup>n</sup>, G. Neugebauer<sup>a</sup>, K. R. Stapelfeldt<sup>l</sup>

<sup>a</sup>Steward Observatory, University of Arizona, 933 N Cherry Ave, Tucson, AZ 85721, USA

<sup>b</sup>Lawrence Berkeley National Laboratory, 1 Cyclotron Road, Berkeley, CA 94720 USA

<sup>c</sup>Spitzer Science Center, 1200 East California Boulevard Pasadena, CA 91125, USA

<sup>d</sup>Steward Observatory, currently at Space Science Institute 4750 Walnut Street, Boulder, Colorado 80301, USA

<sup>e</sup>Ball Aerospace, 1600 Commerce, Boulder, Colorado 80301, USA

<sup>f</sup>Cardiff University, CF10 3XQ, Wales, UK

<sup>g</sup>Steward Observatory, currently at Departamento de Astrofísica Molecular e Infraroja, IEM, CSIC, Serrano 113b, 28006, Madrid

<sup>h</sup>Steward Observatory, currently at Institut d'Astrophysique Spatiale, bât 121, Université Paris-Sud, F-91405 Orsay Cedex, France

<sup>i</sup>University of California, Berkeley, CA, 94720 USA

<sup>j</sup>Michelson Center, California Institute of Technology, Pasadena, CA 91125, USA

<sup>k</sup>Black Forest Engineering 1879 Austin Bluffs Parkway, Black Forest, CO 80907

<sup>l</sup>Jet Propulsion Laboratory, 4800 Oak Grove, Pasadena, CA 91109, USA

<sup>m</sup>Harvard-Smithsonian Center for Astrophysics, 60 Garden Street, Cambridge, MA 02138

<sup>n</sup>National Optical Astronomy Observatories, 950 N. Cherry St., Tucson, Arizona 95719

## ABSTRACT

The Multiband Imaging Photometer for *Spitzer* (MIPS) provides long wavelength capability for the mission, in imaging bands at 24, 70, and 160 $\mu$ m and measurements of spectral energy distributions between 52 and 100 $\mu$ m at a spectral resolution of about 7%. By using true detector arrays in each band, it provides both critical sampling of the *Spitzer* point spread function and relatively large imaging fields of view, allowing for substantial advances in sensitivity, angular resolution, and efficiency of areal coverage compared with previous space far-infrared capabilities. The Si:As BIB 24 $\mu$ m array has excellent photometric properties, and measurements with rms relative errors of 1% or better can be obtained. The two longer wavelength arrays use Ge:Ga detectors with poor photometric stability. However, the use of 1.) a scan mirror to modulate the signals rapidly on these arrays, 2.) a system of on-board stimulators used for a relative calibration approximately every two minutes, and 3.) specialized reduction software result in good photometry with these arrays also, with rms relative errors of less than 10%.

**Keywords:** infrared, space instrumentation, astronomy

## 1. INTRODUCTION

Previous instruments to explore the far-infrared sky have been based on modest numbers of individual detectors rather than true detector arrays. The Infrared Astronomy Satellite (IRAS) had 15 detectors at 25 $\mu$ m, 16 at 60 $\mu$ m, and 15 at 100 $\mu$ m. The demands of an all-sky survey with the IRAS focal plane of discrete detectors resulted in use of individual projected pixels substantially larger than the 60-cm telescope diffraction limit, e.g. 1.5' X 4.5' at 60 $\mu$ m. The ISOPHOT instrument on the Infrared Space Observatory (ISO) had a single detector at 25 $\mu$ m, 9 detectors at 50 to 110 $\mu$ m and 4 from 120 to 200 $\mu$ m. Again, because of the small number of detectors, projected pixel scales were substantially larger than the telescope diffraction limit, for example a center-to-center pixel pitch of 46" at 50 to 100 $\mu$ m. The achieved resolution was typically somewhat larger than the pixel pitch, e.g., ~ 60" at 60 $\mu$ m.

The Multiband Imaging Photometer for *Spitzer* (MIPS) is the first far infrared space astronomy instrument to use true detector arrays -- 128 X 128 pixels at 24 $\mu$ m, 32 X 32 pixels at 70 $\mu$ m, and 2 X 20 pixels at 160 $\mu$ m. In addition to these imaging bands, it provides very low resolution "Spectral Energy Distribution (SED)" spectroscopy from 52 to 100 $\mu$ m. The instrument concept is based on simple principles. One band is set at 70 $\mu$ m in the heart of the far infrared, but not at so long a wavelength as to be overwhelmed by confusion noise (which grows rapidly toward longer far infrared wavelengths due both to the increasing beam size and to the steeply rising source spectra). A second band is placed at 24 $\mu$ m, the logarithmic midpoint between the 70 $\mu$ m band and the longest Infrared Array Camera (IRAC) band at 8 $\mu$ m. The third band is centered at 160 $\mu$ m, roughly the logarithmic midpoint between 70 $\mu$ m and the first submm wavelengths accessible from the ground, 350 and 450 $\mu$ m. The SED mode is to provide a modest measure of spectral information between these bands.

Because the 0.85m aperture makes *Spitzer* "resolution challenged," all bands of MIPS sample the point spread function critically (at 0.4  $\lambda/D$  at 24 and 160 $\mu$ m, 0.3  $\lambda/D$  at 70 $\mu$ m). Thus, the instrument achieves telescope-limited resolution of 6", 18", and 40" respectively at 24, 70, and 160 $\mu$ m. In the case of the 70 $\mu$ m band, critical sampling was expected to exact a significant sensitivity penalty, so a scale change to double the projected pixel size is provided for general use. Through the combination of critical sampling and true, high performance detector arrays, MIPS achieves simultaneously high sensitivity, a large imaging field, and the maximum possible angular resolution, essential both for detailed studies of source structure and to penetrate confusion limits as deeply as possible.

## 2. OVERALL INSTRUMENT DESIGN

The design of MIPS can be understood by reference to Figure 1. Light from the telescope is brought to a focus near two pickoff mirrors, one for the 70 $\mu$ m optical train and one for the 24 and 160 $\mu$ m trains. The pickoff mirrors relay the light to field mirrors at the back of the instrument, which form pupils on facets of a scan mirror. The primary cold baffles for the 70 and 24/160 $\mu$ m optical trains are placed around these facets. From the scan mirror in its center position, the 70 $\mu$ m channel is directed to the detector array for the large-scale imaging mode. In this scan mirror position, the 24 and 160 $\mu$ m channels are relayed to a second image plane, where they are separated and directed to the appropriate arrays. The nominal fields are 5 X 5 arcmin at 24 and 70 $\mu$ m and 0.75 X 5 arcmin (with no detectors in the center row) at 160 $\mu$ m. For the 70 $\mu$ m channel, another scan mirror position directs the light to a reflective slit, from which it goes to a grating and additional mirror that focuses the dispersed spectrum onto the array. Yet another position directs the light into a higher-magnification optical train, with a field of view of 2.5 X 2.5 arcmin. When the scan mirror is in either of these two positions, the 24 and 160 $\mu$ m channels are not used (except possibly for dark current measurement). Heim et al. provide a more detailed description of the instrument design<sup>1</sup>.

MIPS has four operating modes:

*Scan map*, in which the observatory is commanded to scan the sky at a constant rate and the scan mirror executes a reverse sawtooth motion to freeze the images on all three arrays for an integration, and then jumps forward for the next integration. All three bands are measured sequentially as the focal planes are scanned over a given region of sky. In the usual form of scan map, a source is measured 10 times as it transits either the 24 or 70  $\mu$ m array, but only once at

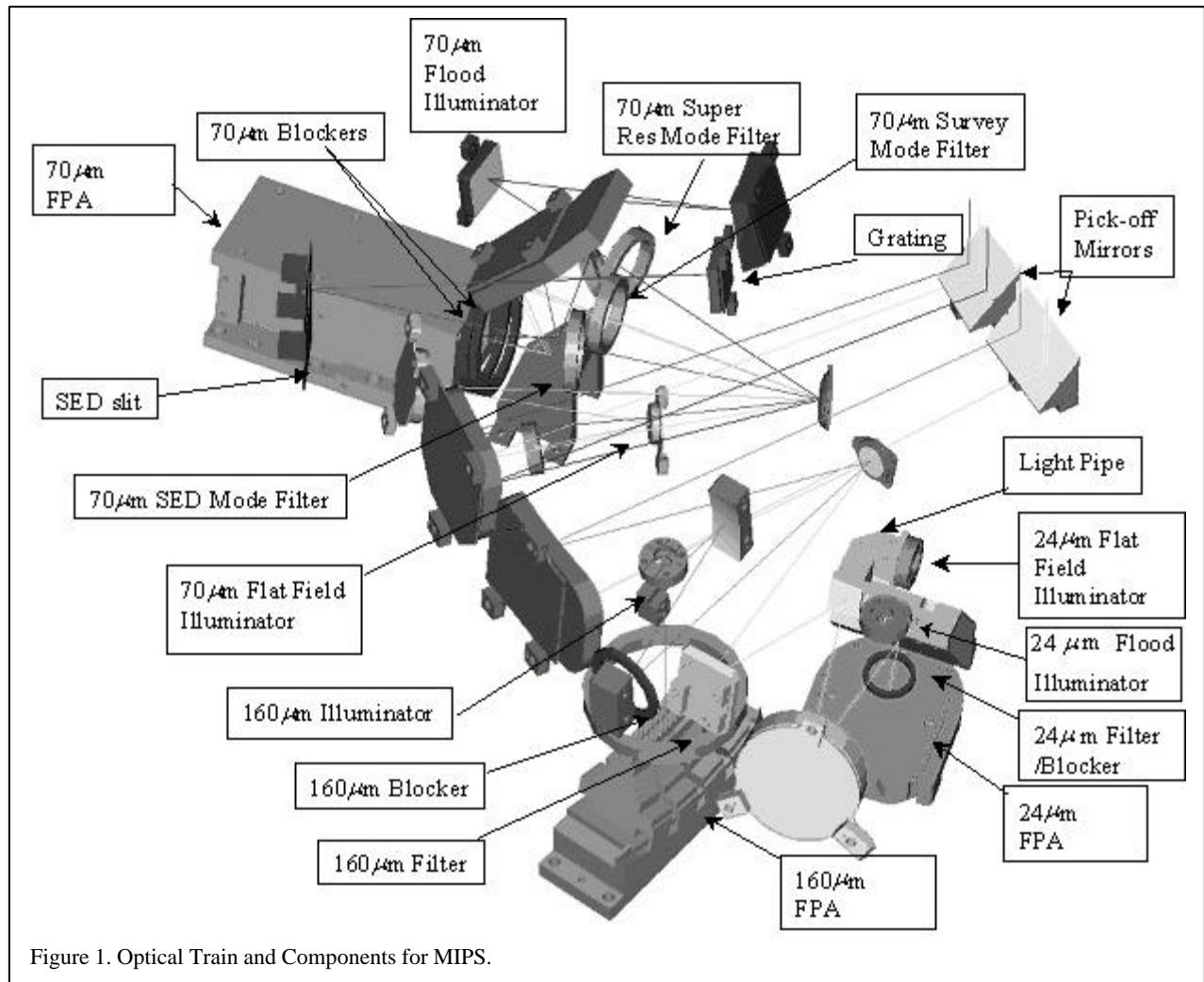


Figure 1. Optical Train and Components for MIPS.

160 $\mu$ m. A high level of redundancy is recommended to remove any spurious effects such as cosmic ray hits, and hence at least a repeat scan is needed for high quality data at 160 $\mu$ m. Stimulator flashes for the germanium arrays are interspersed with sky measurements approximately every two minutes.

*Photometry*, in which the spacecraft points at the object of interest and a combination of scan mirror motions and spacecraft small offsets is used to dither the image on the arrays. A set of 12 measurements is taken as a minimum, bracketed by stimulator flashes for the germanium arrays. In addition, there is a "cluster mode" in which the dithering is largely by spacecraft motions.

*SED*, in which the object image is placed on the slit of the 70 $\mu$ m spectrometer and the scan mirror is used to modulate the spectrum on and off the array.

*Total Power*, in which the scan mirror is used to block the view of the sky for an array to determine the offset level, then to put its view on the sky to measure the total flux.

These modes emphasize a high level of redundancy in the data to allow rejection of outlier signals and to provide more reliable measurements. They also make use of scan mirror motions to provide rapid offsets on the sky without the inefficiencies associated with moving and stabilizing the spacecraft. The integration of these features into the data reduction pipeline is described by Gordon et al.<sup>2,3</sup>.

Under optimum conditions, the  $5\text{-}\sigma$  detection limits on point sources in 500 seconds of integration at 24, 70, and  $160\mu\text{m}$  are 0.11, 6, and 15mJy, respectively. The first is about 1.5 times better and the latter two about 3 times worse than pre-launch estimates. The germanium array sensitivities are degraded by a higher-than-expected rate of large cosmic ray hits. In addition to the photon and read noise, the performance of MIPS is limited by confusion due to the crowding of distant infrared galaxies on the sky<sup>4</sup>. The instrument should reach the confusion limit at 24 and  $70\mu\text{m}$ , defined as  $1\text{-}\sigma$  photon/detector noise equal to  $1\text{-}\sigma$  confusion noise, in integrations of about half an hour. At  $160\mu\text{m}$  this limit is reached in integrations an order of magnitude shorter (matching the factor of ten smaller sky coverage and hence ten times shorter integrations in the mapping mode with the  $160\mu\text{m}$  array).

### 3. OPTICAL DESIGN

The optical components of the instrument are shown in Figure 1. All reflecting optical elements are flats or surfaces of revolution and were diamond turned directly in 6061-T651 aluminum alloy (by II-VI Corporation). The surface microroughness level and wavefront fabrication accuracy required for the MIPS optics are readily met with typical diamond turning processes. Only one surface (in the  $24\mu\text{m}$  band) is required to be aspheric to achieve all design wavefront requirements. The on-orbit performance demonstrates that MIPS is diffraction limited in all bands. Combined with the critical pixel sampling and high level of dithering in the MIPS observing, the resulting images should be highly amenable to deconvolution and model fitting to boost the effective resolution.

The far infrared filters and spectral blockers were supplied by Queen Mary College Industries, under the direction of Peter Ade. They presented a unique challenge because of the large clear apertures required by the instrument design. For many of the filters, this challenge was met by embedding the filter grids in polypropylene sheets, with thin dielectric elements between sheets to maintain the grid spacing. The resulting filter is mechanically rugged and the filters very robust. The filters have excellent out-of-band rejection characteristics. Unfortunately, a scattering path off the  $160\mu\text{m}$  blocker partially negates this feature in that band. The  $24\mu\text{m}$  filter was supplied by Optical Coating Laboratories, Inc. (OCLI) as a standard long-pass dielectric stack. To reduce the number of layers on the filter and hence to make it more robust, no long wavelength cutoff is provided; the instrument depends on the photoconductive edge of the Si:As BIB detectors to limit the response toward long wavelengths. For all bands, blocking filters are mounted close to the front of the detector array to provide a high level of immunity to stray light. These filters are tilted so any ghosts are offset from the primary image. In practice, the filters are of adequately high efficiency that the resulting ghost images are very faint and can be ignored for nearly all observations.

The diffraction grating was ruled directly in aluminum on a diamond turned spherical surface by Hyperfine, Inc. The blaze angle was set at 4.75 degrees. Trades completed between the Code V model and CAD mechanical models finalized the grating at  $\sim 21.3$  mm ruled width and  $\sim 186$  mm surface radius. This gives a total grating surface slope change of 6.6 degrees. Transmission efficiency considerations as well as practicalities of grating manufacture say that the grating surface slope change in a given ruling panel should not exceed the blaze angle. This indicated a two panel ruling for MIPS, providing a peak efficiency of just over 60%. Further, the resolution of multipartite gratings is limited to the total number of ruling lines per panel times the order of use. The resolution achieved by the spectrometer in the geometric limit is very close to  $1.67\mu\text{m}$  per pixel, independent of wavelength. Diffraction degrades the resolution from this value over the long-wavelength half of the spectral range.

The flood and flat field illuminators were manufactured by J. Beeman of Lawrence Berkeley National Laboratory. They are of reverse bolometer type. The emitting elements are sapphire plates about  $40\mu\text{m}$  thick and 1mm square, blackened with a thin, sputtered film of NiCr. This plate is suspended by nylon threads in a mounting ring. Fine brass wires from the ring to the element allow electric current to be passed through the NiCr coating to heat the device.

To reduce the cost and mass of the SPITZER spacecraft, much of the electronics required by the IRS and MIPS are shared, including a warm electronics chassis, power supplies, the instrument processor (RAD6000) and the control and science data interfaces to the spacecraft computer. The IRS instrument has four Si FPAs and MIPS relies on the IRS electronics to control and read out the MIPS Si:As FPA. Two boards designed and built by the MIPS team specifically to control the germanium arrays and the scan mirror are mounted in the common electronics chassis.

The MIPS/IRS warm electronics are designed to be standby redundant; that is, two identical electronics boxes are flown; both boxes are connected to the FPAs and scan mirror in the cold instrument, but only one box is powered at a time. Each circuit that is connected to the cold instrument is designed so when the circuit is not powered it does not load the signal line running from the powered electronics box to the cold instrument. To provide further protection from failures, each Ge FPA is treated as two independent arrays. Independent clock and DC voltages are provided for each 16x32 half of the 70 $\mu$ m FPA as well as each 2x10 half of the 160 $\mu$ m FPA. The scan mirror has redundant motor windings and position sensors. The instrument cabling was designed so no single failure would eliminate an entire instrument function.

The detector arrays and cryogenic scan mirror mechanism are described separately below.

## 4. DETECTOR ARRAYS

### 4.1 Si:As BIB Array Design

At 24 $\mu$ m, Si:As IBC (impurity band conduction) detectors<sup>5</sup> provide high quantum efficiency, low susceptibility to ionizing particles, and good photometric properties. The MIPS 128 X 128 array of these detectors was built by Boeing North America under the leadership of the *Spitzer* Infrared Spectrograph (IRS) team and is identical to the two short wavelength arrays in the IRS<sup>6</sup> except that the MIPS array has a single layer  $\frac{1}{4}$  wave anti-reflection coating of ZnSe, designed for 24 $\mu$ m. The device has four output amplifiers, each of which reads every fourth pixel in a row. That is, the readout is in columns, with an output amplifier for each of columns 1, 2, 3, and 4, repeated for 5, 6, 7, and 8. A somewhat unconventional aspect of the array is that the driver is separated from the detector hybrid and shift registers. The internal source loads and clock buffer circuits are also included with this "satellite chip." Since much of the power dissipated in the device is in the output FET and these other circuits, they are a relatively bright source of glow and this architecture significantly reduces the dark current in the array. In the IRS/MIPS arrays, the detector/source follower/shift register part of the array is mounted on a fiberglass tube for thermal isolation from the instrument baseplate. The detector array is heated above the baseplate temperature to 3 to 7K to improve its performance, particularly by suppressing latent images. The satellite chip is mounted on the array mount sunk to the helium bath. The connections are made across this thermal difference with aluminum (1% silicon) bonding wire that has adequate thermal impedance to support the temperature differential between detectors and satellite chip.

The unit cell is an integrating source follower circuit. With this circuit, the detector is gradually debiased as signal is accumulated. A 10% departure from linearity occurs slightly above 400,000 electrons collected, but the flight electronics saturate at about 320,000 which is the practical limit for the instrument. Signals are brought in and out of the array on a three layer Kapton circuit board that carries filter/protective capacitors, temperature sensors, and similar components. The interface to external cabling is through a connector soldered into the Kapton board.

During evaluation of pre-flight detectors, the IRS team discovered that the devices were subject to damage by ionizing particles, which could activate a high dark current level. It is believed that this effect is caused by damage to the blocking layer that permits conduction by tunneling, since the activated dark current shows little dependence on temperature but a strong dependence on the maximum electric field, which occurs in the blocking layer. Since the field required to deplete the IR active layer is reduced if the minority impurities are kept at a very low concentration in it, relatively radiation-hard arrays can be manufactured if unwanted impurities can be controlled. The IRS/MIPS Si:As detector material was produced at Lawrence Semiconductor Laboratories, which has demonstrated the ability to produce very high purities. The minority concentration in these detectors is well below 10<sup>12</sup> cm<sup>-3</sup>. In addition, the array mount and the design of the MIPS optics provides a minimum shielding of 5 g cm<sup>-2</sup> of aluminum in all directions. Consequently, we do not expect radiation damage to be significant over the *Spitzer* lifetime. In fact, there was virtually no damage - only one pixel was affected - in the large solar storms that occurred during late October and early November, 2003, with a number of days with > 10Mev proton fluxes larger than 1000 cm<sup>-2</sup> s<sup>-1</sup> sr<sup>-1</sup>.

### 4.2 Si:As BIB Flight Detector Performance

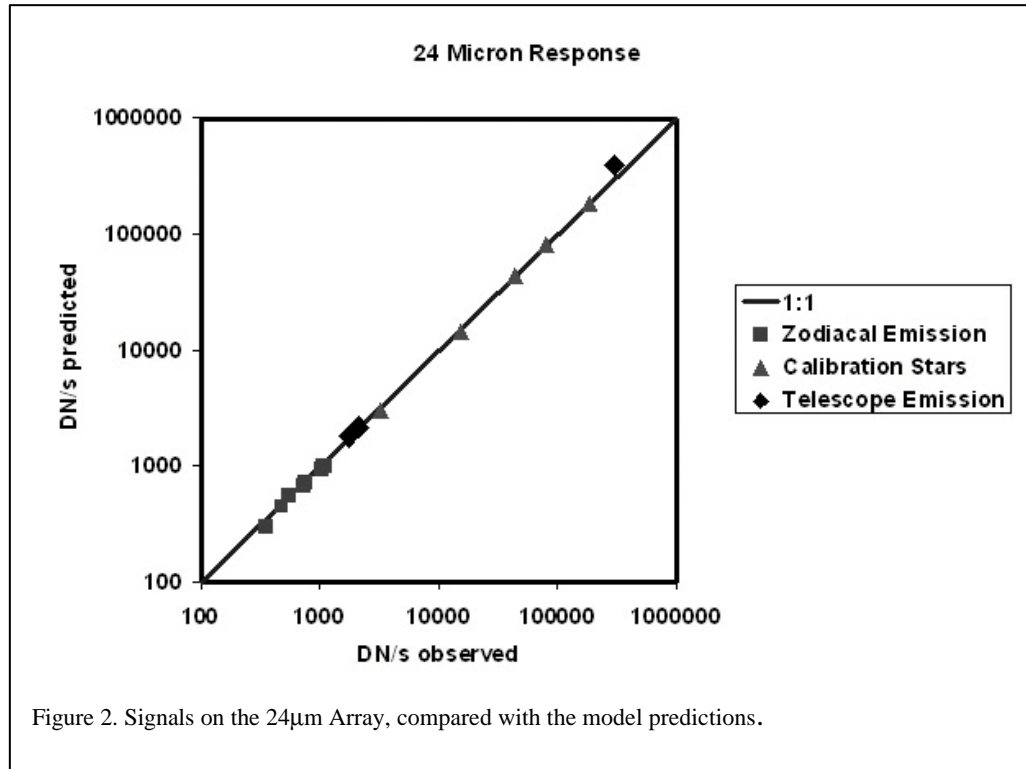


Figure 2. Signals on the 24 $\mu$ m Array, compared with the model predictions.

After initially turning on the Si:As array, it shows a slow drift (~ 30 minutes) to stable operation as well as a pattern of bars in its output. Attaining a good operating equilibrium can be accelerated to virtually instantaneous by annealing the array to ~ 20K. Thereafter, it is very stable and has excellent photometric properties. The on-orbit modeled performance of the array agrees very closely with the preflight measurements. The

operating temperature and optimum bias for the array are set by a number of considerations. A bias of 1.5V allows full depletion of the infrared-active layer but no significant gain in the detector, the optimum operating condition for the relatively high backgrounds in broadband imaging. With this bias, the detective quantum efficiency in the MIPS band is about 63%. The dark current is reduced roughly exponentially with temperature down to about 7.5K, and then transfers to temperature independence at about 3e/s below about 6.5K. To avoid creating a background signal at 160 $\mu$ m, we set the operating temperature at 5.15K. At this temperature, we find that the latent images are 0.7% of the primary image in the first following integration, then decay slowly (timescale of about ten minutes) thereafter. There is a far more persistent latent image when a very bright source is observed. Operation at a lower temperature was shown to increase the latent images substantially and not to reduce the background at 160 $\mu$ m. The array output is sampled twice a second and fitted with a simple least squares algorithm. Under this strategy, the read noise is 40 electrons rms.

At 24 $\mu$ m the photometry repeats to about 1% rms for individual bright sources after all 12 photometry pointings have been combined. The array is stable from observing campaign to campaign, with no significant departure from the within-campaign photometric calibration. Dark and flat field frames are also stable. It was possible to fit the output signals with a radiometric model starting with the telescope at 58K. The model agreed closely with the observed signals as the telescope cooled, and also fitted the signals from standard stars and the diffuse zodiacal emission. This agreement held over three orders of magnitude of signal strength, as shown in Figure 2. Thus, MIPS will open up possibilities for science programs emphasizing an unprecedented level of accuracy in the deep mid-infrared, such as searches for subtle variability, and determining new constraints on stellar atmosphere theory. It also should provide excellent results on extended sources and diffuse emission.

### 4.3 Ge:Ga Array Design

The only high performance detector type for the two longer wavelength bands that operates at the temperature available in the *Spitzer* cryostat is germanium photoconductors<sup>5</sup>. A 32 X 32 Ge:Ga array<sup>7</sup> operates between 50 and 100 $\mu$ m, while a 2 X 20 stressed Ge:Ga device<sup>8</sup> operates at 160 $\mu$ m. The absorption cross sections and maximum impurity concentrations in these materials set the basic boundary conditions for detector geometry, since they yield absorption

lengths of 1 – 3 cm. A number of considerations lead to a need for detector dimensions substantially less than these absorption lengths – among them are the cosmic ray hit rate in space, and the need to control optical cross talk in the detector arrays.

The 70 $\mu$ m array is based on bars of Ge:Ga that are 2mm wide along the direction of photon incidence. At the back of each bar but not in contact with it is a mirror of aluminized sapphire that reflects escaping photons back into the detector. This geometry provides a total path length of 4mm (ignoring additional reflections from the detector front face and the extra path for photons at off-normal incident angles). Each bar is 32 pixels long and the individual pixels are delineated by individual contact pads on the output side of the detectors. A single sheet common contact is deposited on the opposite side. Structure to hold the detector bars is hidden by an optical concentrator, in the form of a wedge of intrinsic germanium that is glued to the detector face. The readouts are fabricated in silicon, using a specialized process developed with Raytheon Vision Systems to allow good DC stability at the detector operating temperature of 1.5K. The detectors operate at small bias voltages. Therefore, the readout circuit is a capacitive trans-impedance amplifier, to maintain the bias accurately on the detector during integrations and to restore it after cosmic ray hits. The readouts are isolated thermally from the detectors, to avoid any potential heating and changes in dark current.

The stressed detectors are 1mm cubes of Ge:Ga mounted in a stressing harness made by electron discharge machining in Aermet 100 steel, which is both exceptionally strong and has a low cryogenic heat capacity. The stress is applied through a leaf spring geometry, so mechanical relaxation of the structure has little effect on the stress level. The area around each detector is enclosed with reflective walls to form an integrating cavity. Signals are brought out of this cavity to a readout similar to those used with the 70 $\mu$ m array. The readout is mounted inside the stressing harness to minimize the lead length to it, and thus to minimize the parasitic capacitances.

These detectors have multiple time constants of response, a rapid one associated with traditional photoconductivity in the bulk of the detector and slower ones associated with the electric field adjustments near the contacts<sup>5</sup>. This behavior is particularly pronounced for the 70 $\mu$ m detectors, because of the shading of the contacts and resulting high impedance and long relaxation time constant for the material near them<sup>9</sup>. The "fast" response is generally better behaved than the "slow" response. The instrument includes a scan mirror to modulate the signals rapidly on the detector arrays, so in many circumstances signals can be extracted in the fast regime.

In addition, the responsivity of these detectors varies unpredictably as they are hit by ionizing particles. MIPS therefore includes reverse bolometer stimulators that are flashed approximately every two minutes during observations to put a controlled calibration signal onto the detectors. Finally, accumulated ionization damage by cosmic ray hits can shift the response characteristics of the detectors and produce excess noise. These effects are removed by heating the detectors from their operating temperatures of 1.5K sufficiently to re-thermalize them (to ~ 5K for the unstressed devices and ~ 3K for the stressed ones).

#### 4.4 Ge:Ga Performance

Performance measurements for the 70 $\mu$ m array both before delivery and during test of the integrated instrument indicated a responsivity of 7 A/W (50mV bias), dark current of ~ 160 e/s, read noise of ~ 120 electrons rms, and pixel operability of 99.6%. For the 160 $\mu$ m array, we found a responsivity of 13A/W (25mV bias), dark current of ~ 500 e/s, read noise of ~ 250 electrons rms, and pixel operability of 100%. Signals repeated to about 1% as measured with reverse bolometer stimulators. Experiments at a cyclotron with a special attenuator to reduce the hit rate to the level expected on-orbit indicated that these performance levels would be approached in space.

However, these performance parameters are degraded in flight. Cable failures in the Spitzer Cryogenic Telescope Assembly (CTA) have reduced the pixel operability through loss of a readout (serving 5 pixels) in the 160 $\mu$ m array and of half the 70 $\mu$ m array plus an additional readout (serving 32 pixels). The overall cosmic ray hit rate is 2 - 3 times higher than predicted, about once per 11 seconds, with some evidence for showering near the array (i.e., simultaneous hits on widely separated pixels). There are many hits by very strongly ionizing particles that upset the stability of the detector/readout combination. To fit the detector behavior in the instrument radiometric model requires assigning read noises for both arrays of about 1000 electrons rms. Due to the effects of cosmic radiation, the responsivities increase steadily after anneals and on average are substantially higher than observed in the laboratory.

The repeatability on the stimulator signals is degraded to 4 - 5%. The overall sensitivity of both bands is degraded about a factor of three compared with pre-launch estimates, but is still extremely good compared with previous far infrared missions.

The far infrared arrays enable a huge advance for infrared astronomy. The per-pixel performance is substantially better than has been achieved previously, and the benefits of critical sampling of the telescope image with true imaging arrays results in a substantial improvement in the achieved resolution as well as the efficiency of observation. On compact sources, high pass filtering of the images can suppress virtually all the artifacts of the slow response component and produce data that is extremely clean, suitable for high signal to noise in long integrations as in Figure 3. For extended sources, such filtering cannot be used but the availability of the scan map mode, in which the field is swept from viewing sky over the source in a relatively rapid manner allows assessment of the artifacts and removal of them to a high degree. The slow signal component at 160 $\mu\text{m}$  has a time constant of order 60 seconds (dependent on background level). As a result, the detectors come to a reasonably good equilibrium on the background emission, and the slow-response artifacts are relatively easily determined. The time constant at 70 $\mu\text{m}$  is much longer (as a result of the transverse contact detector geometry), making mapping of extended sources more challenging; nonetheless, excellent results are being obtained. At 160 $\mu\text{m}$ , the light leak (see Section 3) is small enough that it is only an issue when looking at bright, Rayleigh-Jeans objects. It is also displaced by 2 - 3 pixels from the intended signal, and we find that subtracting a template from the observed point spread function can recover photometry on Rayleigh-Jeans sources with effective signal-to-noise of 2:1 to 3:1. That is, it is plausible to expect to detect a 160 $\mu\text{m}$  excess equal to the photospheric emission of a hot star (a net signal twice the photosphere alone) using this technique. Further improvement may be possible as we gain experience.

A major issue with far infrared Ge:Ga detectors used in previous space

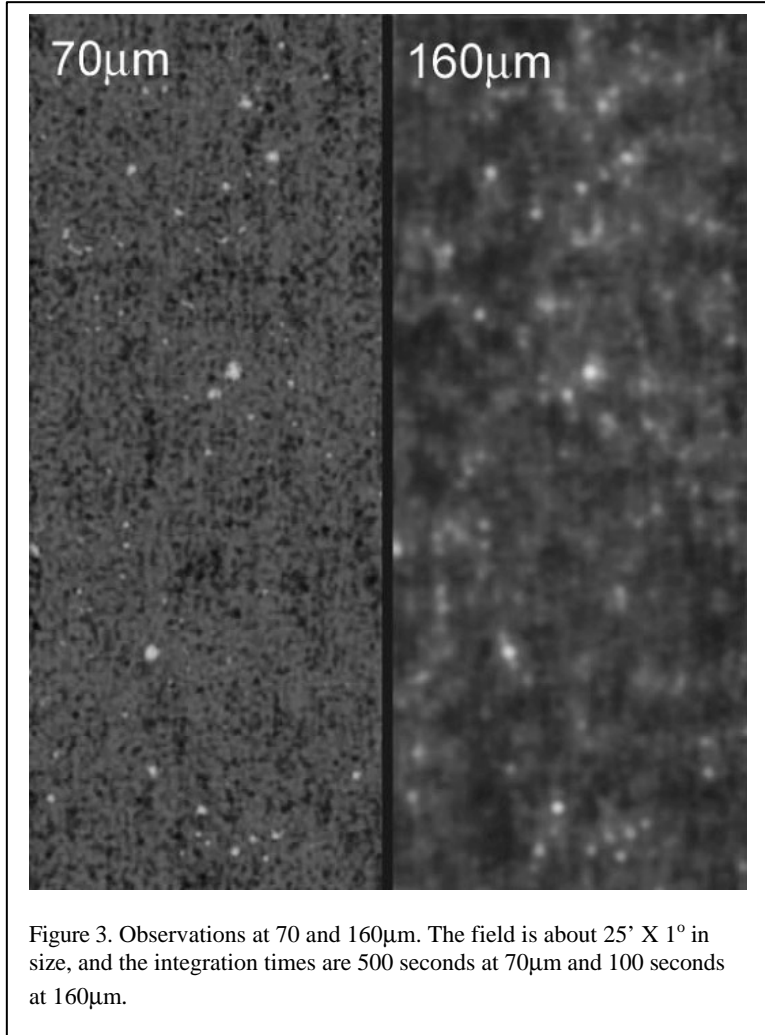


Figure 3. Observations at 70 and 160 $\mu\text{m}$ . The field is about 25' X 1° in size, and the integration times are 500 seconds at 70 $\mu\text{m}$  and 100 seconds at 160 $\mu\text{m}$ .

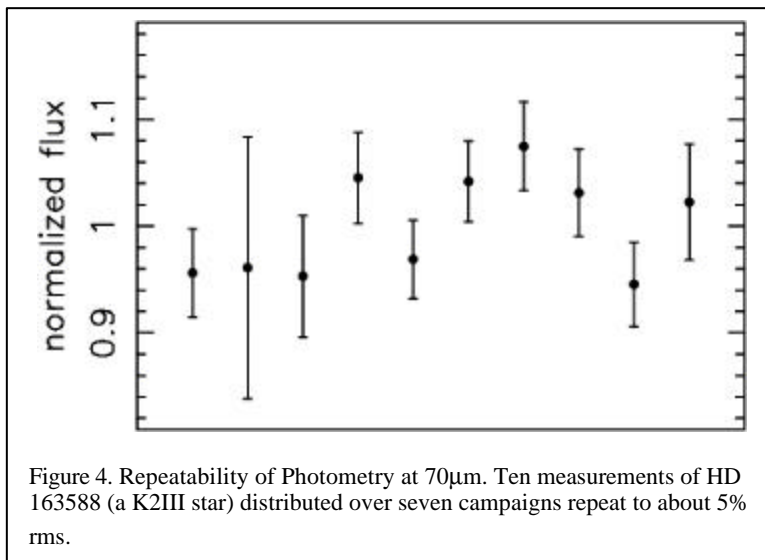


Figure 4. Repeatability of Photometry at 70 $\mu\text{m}$ . Ten measurements of HD 163588 (a K2III star) distributed over seven campaigns repeat to about 5% rms.

missions has been tracking the responsivity shifts to maintain accurate calibration. In MIPS, the frequent calibration with stimulators and the specialized data pipeline<sup>2,3</sup> have yielded excellent photometric performance. For example, Figure 4 shows the accuracy with which photometry of a calibration star repeats. We currently estimate the overall photometric accuracy of the instrument to be about 10%, to allow for variations as a function of background level. The performance in Figure 4 is closer to 5% on a single star, and indicates that photometry approaching this latter level will be possible as the instrument behavior is further characterized.

## 5. CRYOGENIC SCAN MIRROR MECHANISM (CSMM)

The CSMM is based on a design used successfully on the Infrared Space Observatory<sup>10,11</sup>, drawings for which were provided by T. DeGrauw. The original concept was modified to carry two mirrors and to reduce power consumption through use of superconducting wires in the motor coils and a differential impedance position sensor<sup>12</sup>. It pivots the two mirrors around a single axis of rotation over a total range of  $\pm 7.5$  degrees. A linear voice coil motor provides the actuation force. A servo system stabilizes the position at the commanded value.

### 5.1 CSMM Design Overview

The flight scan mirror is illustrated in Figure 5. Its most important properties are: 1.) single axis rotation over a total of  $15^\circ$ ; 2.)  $1^\circ$  step and settle in less than 0.2 sec; 3.) precision of better than 2 arcsec rms; 4.) operating temperature of  $< 2\text{K}$  to  $300\text{K}$ ; 5.) structure of 6061-T651 aluminum, weight 362 grams, size of 63 x 61 x 120mm; and 6.) power dissipation:  $< 0.5\text{mW}$  at  $2^\circ\text{K}$ .

The scan mirror consists of two main sub-assemblies. The fixed portion is made up of the base, frame, magnet, position sensor coils, and housings. The rotating portion is made up of the mirror carrier, position sensor blades, the two mirrors and the coil assembly. Two  $3/16$  inch diameter Lucas Flex Pivots are used

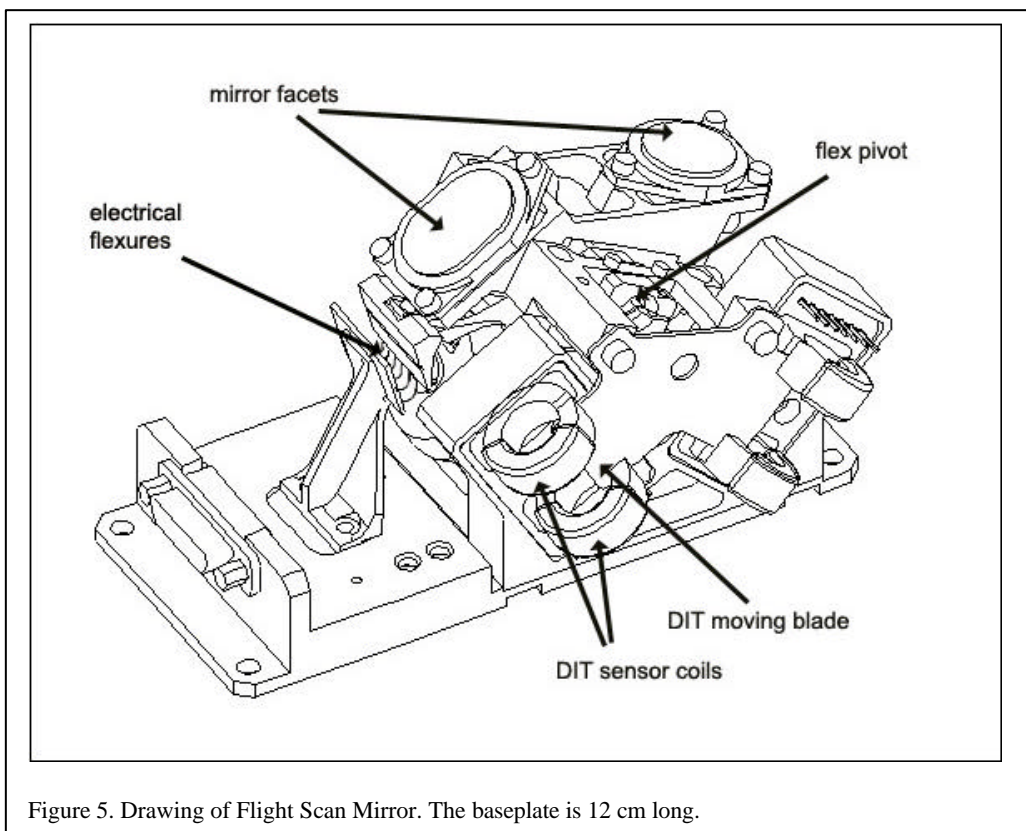
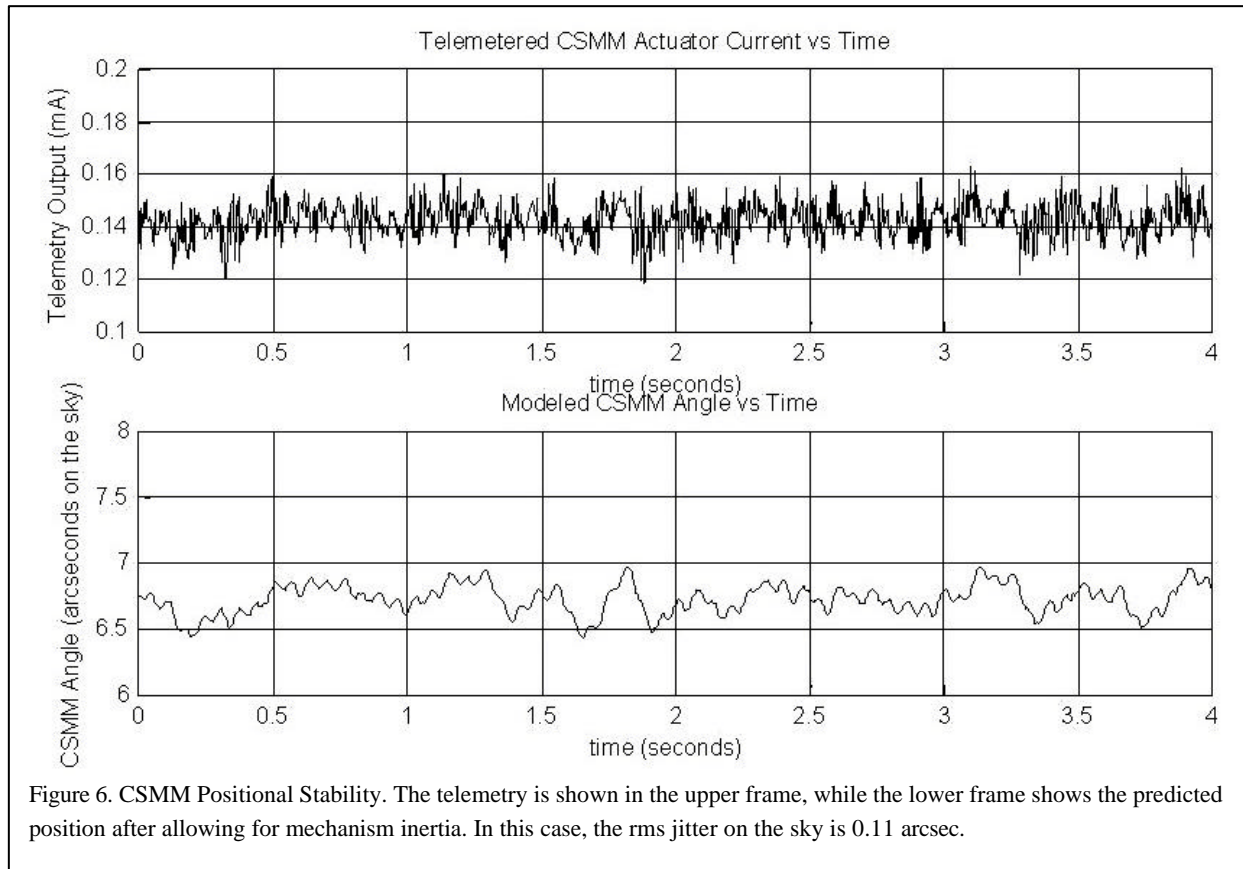


Figure 5. Drawing of Flight Scan Mirror. The baseplate is 12 cm long.

to support the rotating part of the mirror. The rotating mechanism is carefully balanced and the centering torque of the flex pivots keeps it well away from its hard stops under launch loads. Electrical flexures connect power to the voice coil.



## 5.2 Power Dissipation Reduction

To reduce the power dissipation of the CSMM, we modified the ISO design by substituting superconducting wire for the copper wire used in the voice coil actuator. The copper coil in the ISO scan mirror dissipates 0.65mW at the maximum deflection of 7 degrees. The MIPS device uses a superconducting wire manufactured by Supercon. This wire is made up of 54 filaments of a niobium titanium alloy that are supported in a copper matrix. The critical temperature for this wire is about 9.5 Kelvin. The copper in the wire allows the mechanism to be operational at ambient temperature, although the resistance of the coil at this temperature is about 400Ω. Using this wire, power dissipation in the mechanism at maximum deflection when operated below the critical temperature is so small that it is practically unmeasurable.

The ISO scan mirror uses a linear variable displacement transducer (LVDT) to provide position feedback information; this device has a power dissipation of about 350μW. We replaced the LVDT with a differential impedance transducer (DIT)<sup>13</sup>. This device provides slightly reduced position accuracy when compared with the LVDT but with power dissipation of less than 100μW. The DIT relies on a pair of transformers, each wound of ultra-high purity copper on a slotted torroid. Both transformer primaries are fed by a constant amplitude 10KHz sine wave. An aluminum blade, which is attached to the rotating scan mirror, moves in the slots cut in the torroid as shown in Figure 5. The blade is designed such that as the mirror rotates in one direction, the amount of aluminum in the slot for one transformer increases while it decreases for the second transformer. Eddy currents in the aluminum blade cause the coupling between the primary and secondary of the transformer to change relative to the amount of aluminum in the slot. Both of the transformer secondaries are fed to a differential amplifier in the electronics and then demodulated and filtered to produce a signal that is directly proportional to the scan mirror angle.

### 5.3 Performance in Flight Instrument

The short term position stability of the scan mirror was determined by monitoring the output of its position sensor. The sensor output is sampled at a 22 $\mu$ sec interval and there is substantial high frequency noise on it. The mechanical inertia of the moving mechanism is too great for it to respond to this noise. The positional stability was determined by using a model of the mechanism to determine the response to the observed positional output signal. Short term jitter was found to be less than 0.15 arcsec rms projected onto the sky. Figure 6 illustrates the behavior at the center position; the data at +5.4 and -5.4 degrees were not significantly different.

Since the CSMM is controlled by a position servo loop, the position accuracy is determined virtually entirely by the performance of this loop. The sensor is held at a constant temperature (~ 1.5K), so virtually any temperature dependent position errors result from the behavior of the warm electronics that read out the position sensor. Achieving the desired temperature stability was one of the more challenging aspects of developing the CSMM control electronics. As a test of the final stability, we put the electronics in a temperature controlled box. The scan mirror position was monitored by measuring the position of a pinhole source projected from the instrument input focal plane through the instrument onto the 24 $\mu$ m array. The centroiding accuracy was about 0.05 arcsec projected onto the sky. Over a total temperature range of 34C for the electronics cold plate, the change in scan mirror position was about 0.35 arcsec on the sky, i.e., about 0.01 arcsec/degree C. For cold plate temperatures above 0C, the scan mirror position was virtually independent of temperature.

Another cause of instability in the CSMM position is susceptibility to noise on the power to the circuit. EMI/EMC testing showed that the position of the scan mirror was strongly affected by signals at 7.8125kHz on either the supply or return line to the CE, and by some odd harmonics of this frequency. A relatively simple filter of inductors and capacitors proved to reduce the feedthrough effects of the interference near 7.8125 kHz by well over an order of magnitude (to below the detection threshold). The filter also suppressed the overtones. To reduce inrush currents, snubbing diodes were added to the filter circuit.

As determined from the flight imaging performance of the instrument, the CSMM is working extremely well. The images are symmetric and fully diffraction limited for all the instrument imaging modes. Thus, the scan mirror is highly stable for the photometric modes, and its scan rate is very accurately controlled for the scan map mode. One small anomaly has appeared on orbit: there appears to be a small offset that takes values up to  $\pm 0.5$  arcsec. This offset remains constant for extended periods, but tends to change with each cycling of the control electronics on and off, and possibly with downlinks.

## 6. CONCLUSION

The MIPS combines advances in infrared detectors at 20 - 200 $\mu$ m with efficient operations using its scan mirror and a well-developed approach to data calibration and reduction. The instrument system provides a substantial advance in performance over previous missions in the far infrared in sensitivity, angular resolution, and areal coverage, and also in the accuracy with which its data can be calibrated.

## ACKNOWLEDGEMENTS

We thank Ball Aerospace for construction of the instrument, Raytheon Vision Systems (J. Asbrock, A. Hoffman, N. Lum) for developing and manufacturing the far-infrared array readouts, the IRS team for supplying the 24 $\mu$ m array, T. DeGrauw for supplying plans for the ISO SWS scan mirror, and the many others who helped make the *Spitzer* Observatory a reality. Development of MIPS was funded by NASA through the Jet Propulsion Laboratory, subcontract #960785.

## REFERENCES

1. G. B. Heim, M. L. Henderson, K. MacFeely, T. J. McMahon, D. Michika, R. J. Pearson, G. H. Rieke, J. P. Schwenker, D. W. Strecker, C. L. Thompson, R. M. Warden, D. A. Wilson, and E. T. Young, Proc. SPIE

Vol. 3356, Space Telescopes and Instruments V, Pierre Y. Bely; James B. Breckinridge; Eds. p. 985-1000, 1998..

2. K. D. Gordon, et al., PASP, in press, 2004.
3. K. D. Gordon, et al., this volume, 2004.
4. H. Dole, et al. ApJS, in press, 2004.
5. G. H. Rieke, *Detection of Light*, 2<sup>nd</sup> Ed. (Cambridge University Press: Cambridge, U.K., 2003).
6. J. Van Cleve, T. Herter, R. Butturini, G. Gull, J. R. Houck, B. Pirger, J. Schoenwald, SPIE Proceedings Vol 2553, 502-513. 1995.
7. E. T. Young, J. T. Davis, C. L. Thompson, G.H. Rieke, G. Rivlis, R. Schnurr, J. Cadien, L. Davidson, G. S. Winters, K. A. Kormos, Proc. SPIE Vol. 3354, p. 57-65, Infrared Astronomical Instrumentation, Albert M. Fowler; Ed., 1998.
8. R. Schnurr, C. L. Thompson, J. T. Davis, J. W. Beeman, J. Cadien, E. T. Young, E. E. Haller, G. H. Rieke, Proc. SPIE Vol. 3354, p. 322-331, Infrared Astronomical Instrumentation, Albert M. Fowler; Ed., 1998.
9. Haegel, N. M., Schwartz, W. R., Zinter, J., White, A. M., and Beeman, J. W., Appl. Opt., 34, 5748, 2001.
10. Wildeman, K.J., Beintema, D.A., Ploeger, G.R., Snel, D. and Wijnbergen, J.J. "Grating Drive for the Short Wavelength Spectrometer in ISO" *Cryogenics* Vol 27, February, 68-72, 1987.
11. Aalders, J.W.G., Wildeman, K.J., Ploeger, G.R. and Van Der Meij, Z.N. "New Developments with the Cryogenic Grating Drive Mechanisms for the ISO Spectrometers" *Cryogenics* Vol 29, 550-552, 1989.
12. Warden, R. M., Heim, G. B., 32nd Aerospace Mechanisms Symposium, 1998.
13. Downey, C.H., Houck, J.R., Kubitsckek, M.J., and Tarde, R.W. "Arcsecond Grating Drive Mechanism" *Cryogenics* Vol 31, 1030-1037, 1991.